nature communications

Article

https://doi.org/10.1038/s41467-025-64028-3

# Evolution of short trichomes and long hairs on *Nigella* petals through co-option of bHLH and non-*MIXTA* MYB genes

Received: 25 January 2025

Accepted: 2 September 2025

Published online: 18 September 2025

Check for updates

Chunxi Peng[1,2,3,4,5], Xu Yao[1,2,3,5], Xuehao Fu[2,5], Sentao Lyu[1,2,3,4,5], Yi Yuan[2], Hong Liao[2], Xiaofeng Yin[1,2,3], Jie Cheng[1,2,3], Xuan Li[1,2,3,4], Hongzhi Kong[1,2,3,4] ✉ & Hongyan Shan[1,2,3] ✉

Conical cells (CCs), trichomes, and hairs are all protrusive epidermal cells of plants, yet the differences and relationships among them remain largely unclear. Here, we show that the unicellular long hairs (LHs) and short trichomes (STs) on *Nigella damascena* petals differ from CCs in shape, length, number, distribution pattern, relative nuclear size, ploidy level, developmental process, and molecular basis. Specifically, *NidaMIXTA*, an ortholog of the famous CC/trichome identity gene in many species, is involved in CC development but does not affect STs and LHs. The identities of STs and LHs, however, are specified by genes encoding components in the MYB-bHLH-WDR (MBW) complex-*GL2* module. STs, which serve as tiny pillars to prop open the upper and lower petal lips and facilitate pollinators' access to nectar, require the function of *NidaMYB5-1*, *NidaGL3*, *NidaTT8*, and *NidaGL2*, whereas the formation of LHs is determined by *NidaMYB5-1/-2*, *NidaGL3*, and *NidaGL2*. The evolution of STs and LHs from LH-like ancestors in the genus *Nigella*, therefore, was likely caused by independent co-option of the *TT8* and *MYB5-2* genes, respectively, followed by refining of their expression patterns.

Conical cells (CCs), trichomes, and hairs are all protrusive epidermal cells of plants. Because they differ in various ways (e.g., shape, size, number, and patterns of distribution and ornamentation) but can be found on a single petal or petaloid organ, they have fascinated scientists for centuries. Functionally, CCs, which characterize petals of about 80% of angiosperms, can increase color intensity, brightness, and surface hydrophobicity, and provide grip for pollinators[1–3]. Trichomes or hairs on petals or petaloid organs, however, can increase the complexity of these organs and endow them with specialized functions (Supplementary Fig. 1)[4,5]. On the adaxial surface of the labella of *Ophrys* (Orchidaceae), for instance, different types of unicellular trichomes mimic hairs of hymenopteran females and facilitate deceptive pollination[6]. Within the perianth tube of most *Aristolochia* (Aristolochiaceae) species, several types of multicellular trichomes coordinately play roles in trapping, retention, and release of insect pollinators[7]. On petals of many Malvaceae species, unicellular trichomes with different lengths can regulate flower bud shape[8,9]. Exploring the development and evolution of these protrusive cells, therefore, is not only the key to understanding their differences and relationships, but also provides insights into how such specialized surface architectures contribute to key ecological functions.

The molecular mechanisms underlying the formation of petal CCs, trichomes, and hairs have been studied in some species. Key regulators shaping CCs include genes encoding enzymes involved in microtubule organization (e.g., KATANIN, PP2A, SPIKE1, and ROP GTPases), cell wall synthesis (e.g., RHAMNOSE BIOSYNTHESIS 1 [RHM1]), and vacuolino

[1]State Key Laboratory of Plant Diversity and Specialty Crops, Institute of Botany, Chinese Academy of Sciences, Beijing, China. [2]Key Laboratory of Systematic and Evolutionary Botany, Institute of Botany, Chinese Academy of Sciences, Beijing, China. [3]China National Botanical Garden, Beijing, China. [4]University of Chinese Academy of Sciences, Beijing, China. [5]These authors contributed equally: Chunxi Peng, Xu Yao, Xuehao Fu and Sentao Lyu.
✉e-mail: hzkong@ibcas.ac.cn; shanhongyan@ibcas.ac.cn

formation (e.g., RAB5 GTPases)[10–13]. Notably, *MIXTA*-like genes of the MYB family have apparently attracted considerable attention due to their diverse roles in regulating the development of various protrusive cells on petals or petaloid sepals. For instance, the *MIXTA* homologs specify the identity or control the shape of CCs in *Antirrhinum majus* (Plantaginaceae)[14], *Petunia hybrida* (Solanaceae)[15], and *Thalictrum thalictroides* (Ranunculaceae)[16,17]; promote cuticle development on the CC surface in *Arabidopsis thaliana* (Brassicaceae)[18]; or perform both functions in *Phalaenopsis aphrodite* (Orchidaceae)[19]. Additionally, the *MIXTA*-like genes were found to be involved in petal trichome formation, e.g., in *Gossypium hirsutum* (Malvaceae)[8,9]. It is also notable that CCs have been classified as trichomes because they are reminiscent of emerging or arrested trichomes[20–22]. Overexpressing *MIXTA* homologs of *A. majus* and other species in *Nicotiana tabacum* (Solanaceae) converted flat cells into conical shape or trichomes[15–17,23]. Consequently, it has been hypothesized that CCs and trichomes may share a common developmental pathway, where the relative timing of *MIXTA* expression specifies fates of the two cell types[23,24].

Notably, apart from *MIXTA*-like genes, other genes have been identified as critical determinants of trichome or hair formation on leaves, seeds, or fruits in species including *A. thaliana*, *G. hirsutum*, *G. arboreum*, *Solanum lycopersicum* (Solanaceae), and *Cucumis sativus* (Cucurbitaceae)[25,26]. For instance, in *A. thaliana*, the leaf trichome fate is determined by a MYB-bHLH-WDR (MBW) protein complex-*GLABRA2* (*GL2*, a class IV HD-Zip gene) module, in which the MYB protein is represented by GLABROUS1 (GL1), bHLH by GLABRA3 (GL3) and ENHANCER OF GLABRA3 (EGL3), and WDR by TRANSPARENT TESTA GLABRA1 (TTG1)[27–31]. Whether genes of these lineages or families contribute to petal trichome specification remains to be investigated. In addition, it has been shown that petal CCs vary in overall size, steepness and height of the cone, base shape, and surface decoration[2], and that petal trichomes can be unicellular or multicellular, straight or curly, long or short, glandular or non-glandular (Supplementary Fig. 1). However, due to the lack of comprehensive studies from an evolutionary developmental perspective, how different types of protrusive cells have evolved on petals in a certain lineage remains poorly understood. Clearly, these limitations have hindered our understanding of the differences and relationships of protrusive cells on petals and petaloid organs.

The genus *Nigella* (Ranunculaceae) appears to be an excellent system for addressing the above issues, for four reasons. First, petals of all *Nigella* species, excluding the three basal species, bear three types of unicellular protrusive cells, i.e., CCs, short trichomes (STs), and long hairs (LHs), each type displaying a unique spatial distribution[32]. For example, on petals of *N. damascena*, CCs are distributed on the adaxial epidermis of lower lip lobes, STs are densely packed on the contact surfaces between upper and lower lips, and LHs are sparsely distributed on pseudonectaries and the adaxial side of lower lip lobes (Fig. 1a). The coexistence of CCs, STs, and LHs on petals provide an opportunity for a direct comparison of these protrusive cell types in one system. Second, it has been shown that noticeably differentiated LHs and STs evolved after *N. integrifolia* split from all other extant species of *Nigella*, and that CCs originated later in the genus[32]. Therefore, a comparison between species with CCs, STs, and LHs (e.g., *N. damascena*) and the basalmost species with only one type of hair (i.e., *N. integrifolia*) allows us to explore the molecular mechanisms underlying the evolution of these protrusive cells in *Nigella*. Third, previous studies speculated that STs may serve at least three functions: filtering pollen grains adhering to the insect proboscis, preventing nectar from drying out, and protecting nectar from being stolen by unfavorable visitors[32,33], implying that STs represent an adaptive character. And fourth, several species in this genus have been developed into model systems, to which virus-induced gene silencing (VIGS), other molecular techniques, and phenotype-controlled pollination experiments are applicable[34–37]. These advantages enable detailed gene expression and functional studies, even the precise assessment of ecological functions for a specific protrusive cell type on petals.

In a previous study, a class I HD-Zip gene, i.e., *LATE MERISTEM IDENTITY1* (*LMI1*) from *N. damascena*, was found to be indispensable for the development of STs on petals; knockdown of it led to the disappearance of STs, but did not affect the development of LHs and CCs[36], implying that different regulatory mechanisms may underlie the formation of STs and the other two protrusive cells. Here, we use petals of *N. damascena* and *N. integrifolia* as research systems and conduct extensive micromorphological, anatomical, cytological, comparative transcriptomic, expression, functional, pollination, and phylogenetic studies. We attempt to explore the cellular features and underlying developmental bases of CCs, STs, and LHs; to understand the ecological functions and evolutionary mechanisms of STs and LHs in *Nigella*; and eventually to disentangle the differences and relationships among CCs, STs, and LHs.

## Results

### Cellular features of CCs, STs, and LHs on *N. damascena* petals

To gain more insights into the cellular features of CCs, STs, and LHs on mature petals of *N. damascena*, we conducted micromorphological, anatomical, and cytological observations (Fig. 1, Supplementary Fig. 2 and Supplementary Data 1). We found that CCs are covered with grainy cuticular striations, whereas STs possess smooth surfaces and LHs show slightly textured cuticular surfaces (Fig. 1a and Supplementary Fig. 2a). We also found that, on each petal, CCs are obviously the highest in number and the shortest in length among the three cell types (Fig. 1a–d). The median number of STs per petal (432) is almost eight times that of LHs (55), whereas the median length of STs (101.55 μm) is only one-tenth that of LHs (1180.48 μm) (Fig. 1j, k). Propidium iodide (PI) and 4′,6-diamidino-2-phenylindole (DAPI) staining indicated that nuclei of CCs showed sizes comparable to those of flat pavement cells (PCs) on petals and guard cells (GCs) on leaves, which are generally believed to have a 2C DNA content[38] (Fig. 1f–i, Supplementary Fig. 2b–i and Supplementary Data 1). In contrast, the nuclear sizes of STs (median volume: 2572.37 $\mu m^3$) are approximately twice those of CCs (median volume: 1373.71 $\mu m^3$) and PCs (median volume: 1213.08 $\mu m^3$), while the nuclear sizes of LHs (median volume: 4622.63 $\mu m^3$) are about twice those of STs (Fig. 1l, m and Supplementary Data 1). Flow cytometry analysis further revealed that while the majority of cells were 2C in samples containing STs and LHs, clear peaks at 4C and 8C levels were detectable (Supplementary Fig. 2j–l), suggesting that endoreduplication occurs in STs and LHs. Taken together, these findings suggest that the CCs, STs, and LHs on *N. damascena* petals significantly differ in shape, length, number, distribution pattern, surface ornamentation, relative nuclear size, and possibly ploidy level.

### Identification of candidate genes for CC, ST, and LH formation

To understand how CCs, STs, and LHs are formed, we first investigated their morphological changes during the development of *N. damascena* petals. We found that LHs start to emerge at stage 6 (S6), then gradually elongate, and stop growing at S12, whereas STs arise at S10 and reach final lengths at S12, and CCs become distinguishable at S11 (Fig. 2a, Supplementary Fig. 3a and Supplementary Data 1). We then examined digital gene expression (DGE) profiles across eight petal stages[36] and in four parts of petals at S10 (Fig. 2c) to identify potential genes involved in the formation of CCs, STs, and LHs. We particularly focused on genes homologous to those involved in CC and trichome/hair development in model plants (Supplementary Data 2). By correlating gene expression dynamics with developmental processes and distribution patterns of CCs, STs, and LHs, we identified five genes that may specify these cells (Fig. 2b, d). *NidaGL1-1* (a R2R3 MYB gene) was expressed at very early stages (S4 and S5), likely only regulating the

https://doi.org/10.1038/s41467-025-64028-3

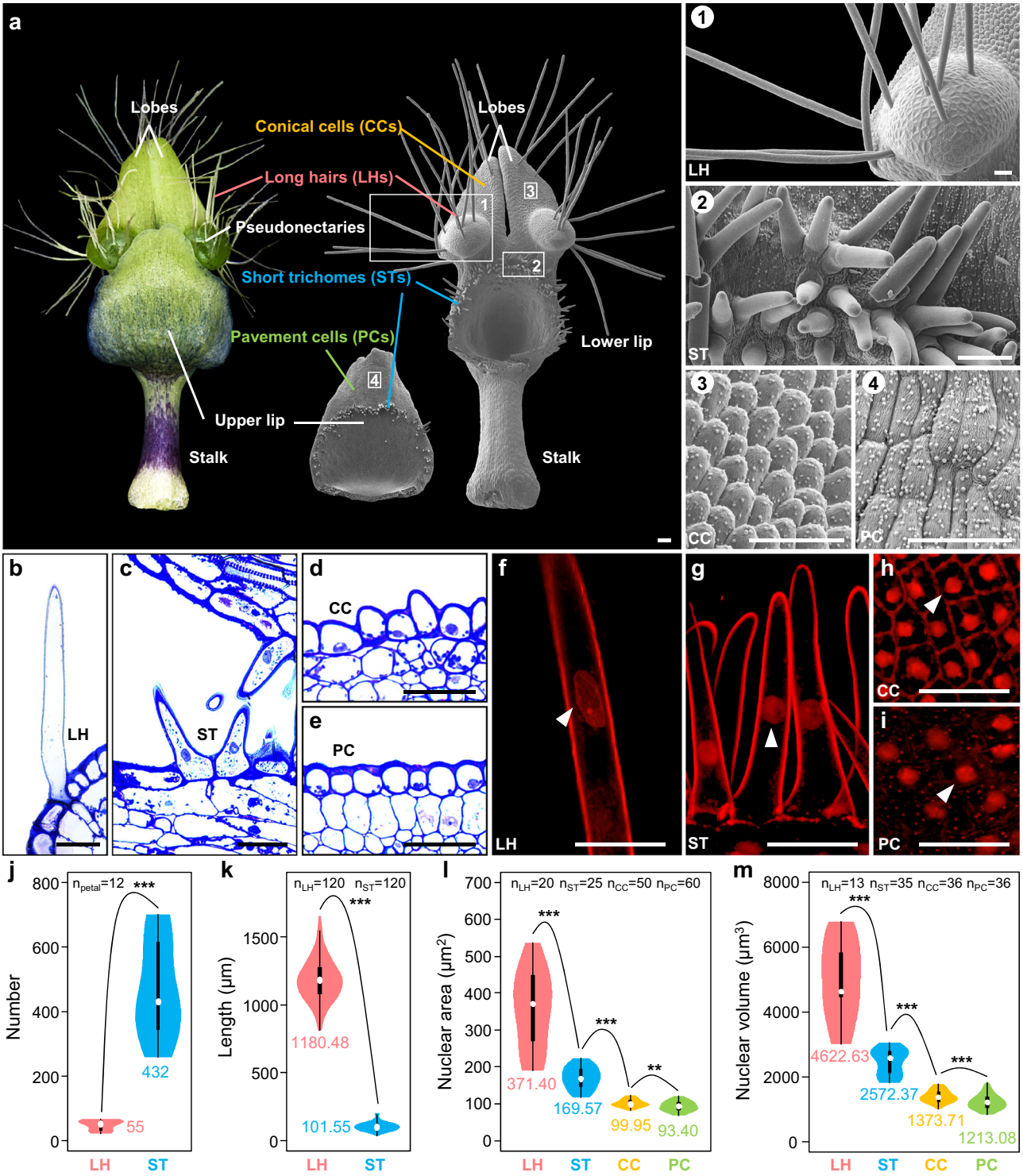


**Fig. 1 | Cellular features of conical cells, short trichomes, and long hairs on *Nigella damascena* petals. a** The distribution of different cell types on a mature petal under stereomicroscope and scanning electron microscope. Numbered regions (1–4) are magnified to show the micromorphology of long hairs (LHs), short trichomes (STs), conical cells (CCs), and pavement cells (PCs), respectively. **b**–**e** Semi-thin sections of regions containing LHs, STs, CCs, and PCs. **f**–**i** Propidium iodide (PI) staining of the four cell types. The white arrowhead points to the nucleus. Scale bars: (**a** left) 100 μm; (**a** right and **b**–**i**) 50 μm. **j** Total numbers of STs and LHs on each petal. **k** Lengths of STs and LHs. **l** The largest PI fluorescence areas of nuclei in the four cell types. **m** Volumes of reconstructed three-dimensional nuclei in the four cell types. In (**j**–**m**), violin outline width shows the density of the data; the thick bar represents the interquartile range (IQR) between the first and third quartiles, with the median marked by a white dot and labeled with the corresponding value; whiskers extend up to 1.5 times the IQR. $^{**}P < 0.01$, $^{***}P < 0.001$ (two-sided Mann-Whitney *U* test). Source data for (**j**–**m**) are provided in Supplementary Data 1. See also Supplementary Fig. 2.

https://doi.org/10.1038/s41467-025-64028-3

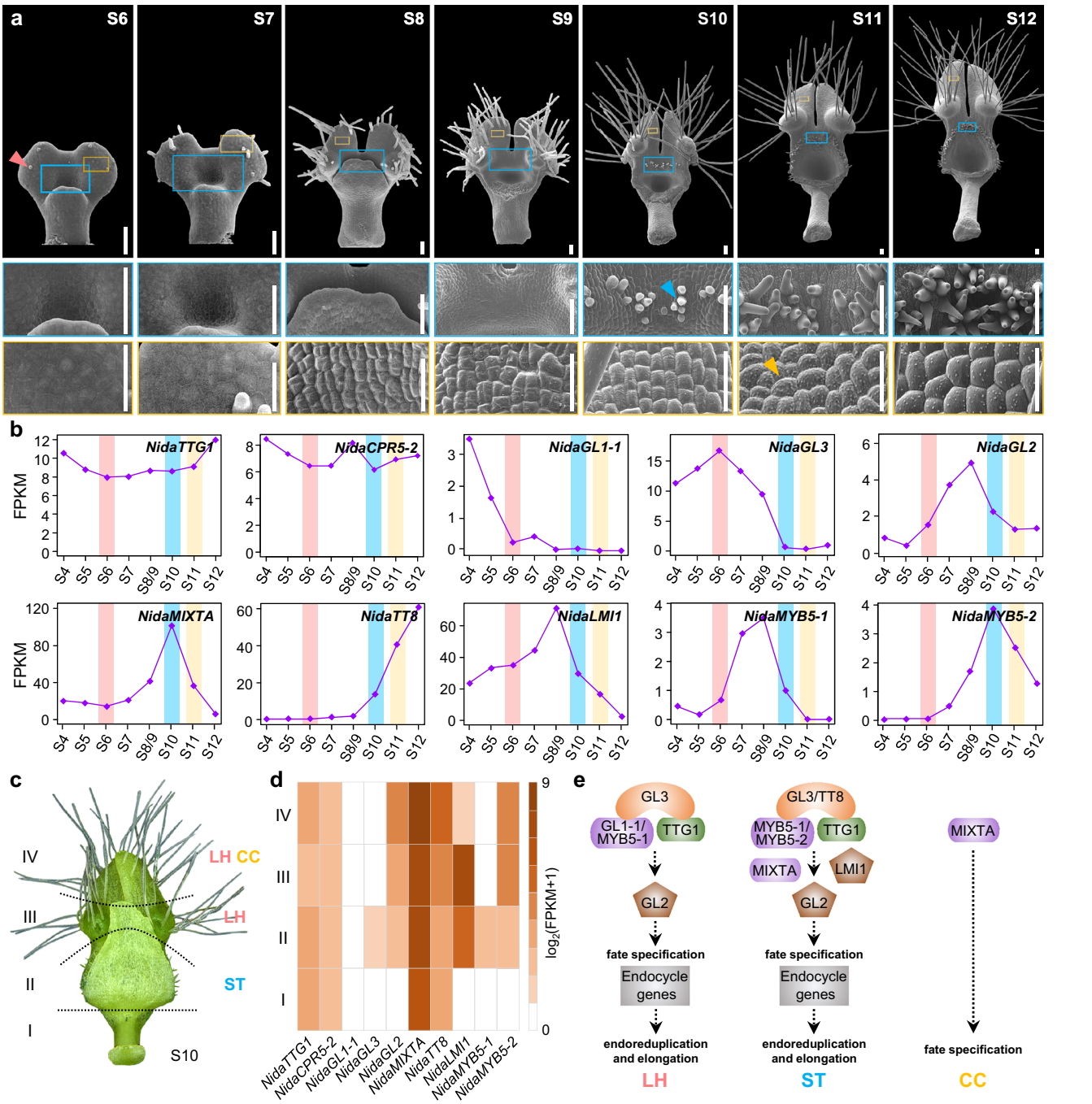


**Fig. 2 | Development processes of conical cells, short trichomes, and long hairs as well as expression profiles of key candidate genes in *Nigella damascena* petals. a** The development of long hairs (LHs), short trichomes (STs), and conical cells (CCs). Images below petals show magnified views of the boxed regions containing STs (sky blue) and CCs (yellow). Red, sky blue, and yellow arrowheads point to the emerging LH, ST, and CC, respectively. For each stage, at least 5 petals were observed. Scale bars: (Rows 1 and 2) 100 μm; (Row 3) 50 μm. **b** Expression profiles of key candidate genes across eight developmental stages of petals. Red, sky blue, and yellow bars indicate the stages when LHs, STs, and CCs arise, respectively. **c** Sampling strategy for the digital gene profiling of the S10 petal. I, II, III, and IV represent four sampled parts. **d** Expression profiles of key candidate genes in the four parts of the S10 petals. Note that in (**b**) and (**d**), except *NidaCPR5-2*, which is a nuclear replication activator candidate, all other genes are candidates for CC or trichome specification. For expression profiles of other candidates, see Supplementary Fig. 3. Source data for (**b**) and (**d**) are provided in Supplementary Data 2. **e** A hypothetical model showing genes involved in the formation of LHs, STs, and CCs. The interaction and regulatory relationships among proteins of candidate genes are illustrated in reference to *Arabidopsis thaliana*. Note that the broadly expressed TTG1 is shown in the model as a potential partner of GL1/MYB5-1/MYB5-2 and GL3/TT8.

initiation of LHs. *NidaGL3* (a bHLH gene) was highly expressed at S6 and specifically expressed in the ST-containing Part II of S10 petals, whereas *NidaGL2* (a class IV HD-Zip gene) was expressed from S6 to S12 and in regions containing both STs and LHs of S10 petals, indicative of their roles in regulating the initiation or development of both STs and LHs. *NidaMIXTA* (a R2R3 MYB gene) showed an expression peak at S10 and was preferentially expressed in the CC-containing Part IV, matching the initiation of STs and the differentiation of CCs, respectively. *NidaTT8* (a bHLH gene) started to be highly expressed from S10, hinting at a specific role in promoting the initiation of STs. In addition, we found seven genes that likely regulate the progression and termination of endoreduplication in STs and LHs, including five potential

activators, i.e., *NidaCONSTITUTIVE EXPRESSION OF PR GENES 5-1* (*NidaCPR5-1*), *NidaCPR5-2*, *NidaROOT HAIRLESS 2* (*NidaRHL2*), *NidaHYPOCOTYL6* (*NidaHYP6*), and *NidaCELL CYCLE SWITCH PROTEIN 52 A1* (*NidaCCS52A1*), which showed relatively higher expression during elongation of LHs and STs; and two potential inhibitors, i.e., *NidaGT-2-LIKE1-1* (*NidaGTL1-1*) and *NidaGTL1-2*, which started to be highly expressed at late stages (Fig. 2b, d and Supplementary Fig. 3b, c).

To identify additional candidate genes, we checked the previously identified stage-specific coexpression modules containing *NidaGL1-1*, *NidaGL3*, *NidaGL2*, *NidaMIXTA*, *NidaTT8*, and *NidaLMI1*[36]. By examining the top 10 transcription factors in each module (Supplementary Data 2), we noticed that *NidaGL2* and *NidaLMI1* were coexpressed with a R2R3 MYB family member, *NidaMYB5-1*. Additionally, *NidaMYB5-1* was specifically expressed in the ST-containing Part II of S10 petals and spatially coexpressed with *NidaGL3* (Fig. 2b, d), strongly implying the involvement of *NidaMYB5-1* in the formation of both STs and LHs. Interestingly, the paralogous gene of *NidaMYB5-1*, *NidaMYB5-2*, was expressed later than *NidaMYB5-1* and showed an expression peak at S10, indicating its role in regulating the development of STs. By taking all the findings into account, we hypothesized that CCs are specified by *NidaMIXTA*, STs by *NidaLMI1*, *NidaMIXTA*, *NidaMYB5-1*, *NidaMYB5-2*, *NidaGL3*, *NidaTT8*, and *NidaGL2*, and LHs by *NidaGL1-1*, *NidaMYB5-1*, *NidaGL3*, and *NidaGL2* (Fig. 2e).

### Expression patterns and functions of *NidaMIXTA*, *NidaGL1-1*, *NidaGL2*, and *NidaGL3*

To test our hypothesis, and more importantly, to understand the relationships among CCs, STs, and LHs, we conducted detailed expression and functional studies for the aforementioned genes in *N. damascena* using mRNA in situ hybridization and VIGS techniques. We started with the well-known *MIXTA*-, *GL1*-, *GL2*-, and *GL3*-like genes. According to our hypothesis, *NidaMIXTA* likely regulates the differentiation of both CCs and STs, and *NidaGL1-1* may be involved in the formation of LHs. However, we found that *NidaMIXTA* was mainly expressed on the adaxial surface of lower lip lobes at S10 and S11, but not in the region producing STs during petal development (Fig. 3a and Supplementary Fig. 4a). Compared with mock (Fig. 3d), knockdown of *NidaMIXTA* did not affect the shapes of CCs and STs, but rather led to a relatively smooth surface of CCs due to the defect in cuticle development (Fig. 3e, Supplementary Fig. 4b–f and Supplementary Data 3). For *NidaGL1-1* and its paralog *NidaGL1-2*, no in situ hybridization signal was observed in protrusive cells on petals at different stages (Supplementary Fig. 5); and no observable phenotypic change was detected on petals of TRV2-*NidaGL1-1*-, TRV2-*NidaGL1-2*-, and TRV2-*NidaGL1-1*-*NidaGL1-2*-treated plants (Supplementary Fig. 6 and Supplementary Data 3). These results strongly suggest that *NidaMIXTA* is only involved in the differentiation of CCs by promoting cuticular modifications, whereas *NidaGL1-1* is not involved in the formation of LHs.

In contrast, in situ hybridization and VIGS results of *NidaGL2* and *NidaGL3* well supported our prediction of their roles in the development of STs and LHs. *NidaGL2* was first expressed in emerging and developing LHs on S6 and S7 petals, and subsequently restricted to nascent and growing STs on petals at S9 and later stages (Fig. 3b and Supplementary Fig. 7a). When *NidaGL2* was downregulated, both STs and LHs became significantly fewer and shorter. On petals with strong phenotypic changes, LHs were generally less than 200 μm, and most STs ranged from 3 to 30 μm (Fig. 3f, Supplementary Fig. 7c, d, g and Supplementary Data 3). On petals showing moderate phenotypic changes, the lengths of most STs and LHs were reduced to about half of those on mock petals (Supplementary Fig. 7e and Supplementary Data 3). *NidaGL3* showed broader expression domains than *NidaGL2*. At early stages of petal development, *NidaGL3* was strongly expressed in epidermal cells on the adaxial side of both upper and lower lips at S6 and then confined to emerging LHs at S7. Later, *NidaGL3* was specifically expressed in the areas where STs would initiate and on the adaxial surface of the upper lip at S9 and S10 (Fig. 3c and Supplementary Fig. 7b). When *NidaGL3* was knocked down, petals with strong phenotypic changes became balder than *NidaGL2*-knocked-down petals: LHs completely disappeared, whereas STs were noticeably reduced in both number and length (generally less than 20 μm) (Fig. 3g, Supplementary Fig. 7c, d, h and Supplementary Data 3). On petals showing moderate phenotypic changes, LHs were almost absent, and STs were fewer and shorter (mostly 20–60 μm) than those on mock petals (Supplementary Fig. 7f and Supplementary Data 3). Taken together, these results indicate that *NidaGL2* and *NidaGL3* indeed promote the formation of STs and LHs.

### Expression patterns and functions of *NidaTT8* and *NidaMYB5*s

We next focused on the remaining candidates, i.e., *NidaTT8* and *NidaMYB5*s. *NidaTT8* was a candidate for the specification of STs. In accordance with our hypothesis, *NidaTT8* was expressed in STs of petals at S10 and later stages (Supplementary Fig. 8a). When *NidaTT8* was knocked down, STs were missing or became extremely short (generally less than 40 μm) on petals with strong phenotypic changes (Fig. 4a, Supplementary Fig. 9a, b, h and Supplementary Data 3); relatively few and short STs (mostly 30–70 μm) were observed on petals showing moderate phenotypic changes (Supplementary Fig. 9c and Supplementary Data 3). Besides, simultaneous knockdown of *NidaTT8* and its paralog *NidaGL3* led to the complete absence of both STs and LHs (Fig. 4b, Supplementary Fig. 9b, d, i and Supplementary Data 3). Interestingly, we found that *NidaTT8* was also expressed in the adaxial side of the upper lip and the abaxial side of the lower lip (Supplementary Fig. 8a). Knockdown of *NidaTT8* alone or in combination with *NidaGL3* affected pigmentation, resulting in green petals (Supplementary Fig. 9e–g). These results indicate that *NidaTT8* not only promotes the initiation of STs redundantly with *NidaGL3* but also regulates anthocyanin biosynthesis on petals.

Our hypothesis stated that *NidaMYB5-1* was a candidate for both STs and LHs, whereas *NidaMYB5-2* for STs only. As expected, *NidaMYB5-1* was first expressed in emerging LHs on S7 petals, and then in ST precursors on S9 petals (Supplementary Fig. 8b). However, we found that *NidaMYB5-2* was specifically expressed in developing LHs from S7 to S10, but not in STs (Supplementary Fig. 8c), against our prediction. When *NidaMYB5-1* was knocked down, STs completely disappeared and LHs were reduced in length (ranging from 100 to 500 μm) on petals with strong phenotypic changes (Fig. 4c, Supplementary Fig. 10a, b, e and Supplementary Data 3), whereas a few STs arose sporadically on petals with moderate phenotypic changes (Supplementary Fig. 10c and Supplementary Data 3). Knocking down *NidaMYB5-2* alone resulted in normal petals (Fig. 4d, Supplementary Fig. 10a, b and Supplementary Data 3). However, in TRV2-*NidaMYB5-1*-*NidaMYB5-2*-treated plants, petals with strong phenotypic changes became nearly glabrous, on which LHs almost disappeared and STs were completely missing (Fig. 4e, Supplementary Fig. 10b, f and Supplementary Data 3). On petals with moderate phenotypic changes, LHs were significantly fewer and shorter than those on the mock petals, and STs were absent (Supplementary Fig. 10d and Supplementary Data 3). These findings indicate that *NidaMYB5-1* not only regulates the initiation of LHs redundantly with *NidaMYB5-2*, but also is responsible for the formation of STs.

To understand how the above functionally characterized genes cooperatively regulate the formation of STs and LHs, we examined the possible regulatory relationships among them. Through qRT-PCR assays, we found that when genes encoding the potential components of the MBW complex, e.g., *NidaMYB5-1*, *NidaGL3*, and *NidaTT8*, were downregulated, the expression level of *NidaGL2* significantly decreased, indicating that *NidaGL2* functions downstream of the hypothetical MBW complex to specify STs and LHs (Supplementary Fig. 11a–c, e). We also found that when the ST-specific gene *NidaLMI1* was knocked down (Fig. 4f), *NidaMYB5-1*, *NidaGL3*, and *NidaGL2* were

https://doi.org/10.1038/s41467-025-64028-3

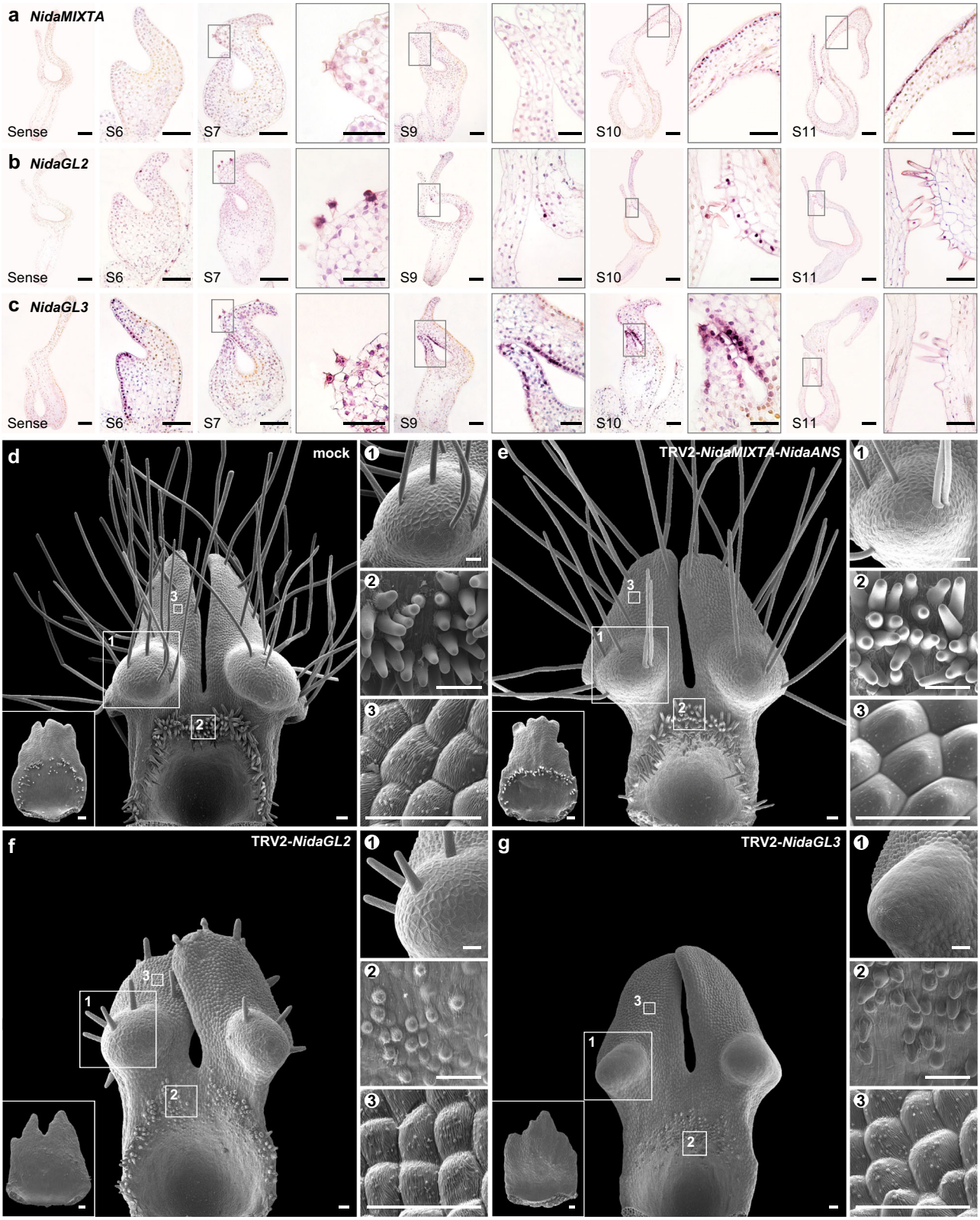


**Fig. 3 | Expression patterns and functions of *NidaMIXTA*, *NidaGL2*, and *NidaGL3*.** **a**–**c** Results of mRNA in situ hybridization for *NidaMIXTA* (**a**), *NidaGL2* (**b**), and *NidaGL3* (**c**) in *Nigella damascena* petals at different stages. For each gene, the first image shows the result using the sense probe. All results are representative of at least two independently repeated experiments. **d**–**g** The morphology and micromorphology of the mock petal (**d**, $n_{petal} = 7$) and petals with strong phenotypic changes in TRV2-*NidaMIXTA*-*NidaANS*- (**e**, $n_{petal} = 3$), TRV2-*NidaGL2*- (**f**, $n_{petal} = 6$), and TRV2-*NidaGL3*- (**g**, $n_{petal} = 10$) treated plants. In each treatment, both the adaxial side of the lower lip and the abaxial side of the upper lip (at the bottom left) are shown. Numbered regions (1–3) are magnified to show phenotypes of long hairs, short trichomes, and conical cells, respectively. Scale bars: (**a**–**c**) 100 μm; (**d**–**g**) 50 μm. See also Supplementary Figs. 4, 7 and Supplementary Data 3.

https://doi.org/10.1038/s41467-025-64028-3

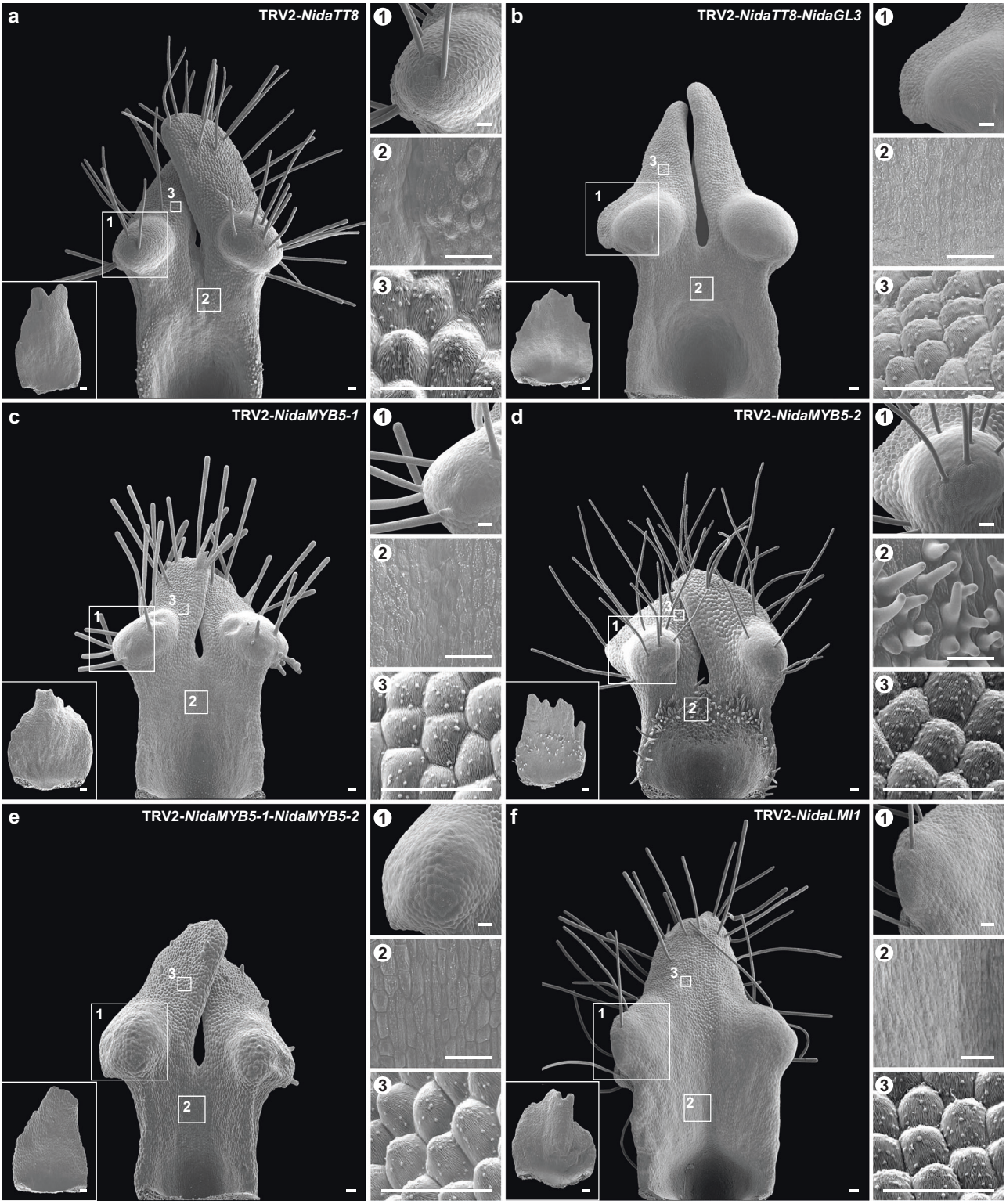


**Fig. 4 | Functions of *NidaTT8, NidaMYB5-1, NidaMYB5-2,* and *NidaLMI1*.** **a**–**f** The morphology and micromorphology of *Nigella damascena* petals with strong phenotypic changes in TRV2-*NidaTT8*- (**a**, $n_{petal} = 6$), TRV2-*NidaTT8-NidaGL3*- (**b**, $n_{petal} = 4$), TRV2-*NidaMYB5-1*- (**c**, $n_{petal} = 3$), TRV2-*NidaMYB5-2*- (**d**, $n_{petal} = 7$), TRV2-*NidaMYB5-1-NidaMYB5-2*- (**e**, $n_{petal} = 3$), and TRV2-*NidaLMI1*- (**f**, $n_{petal} = 4$) treated plants. In each treatment, both the adaxial side of the lower lip and the abaxial side of the upper lip (at the bottom left) are shown. Numbered regions (1–3) are magnified to show phenotypes of long hairs, short trichomes, and conical cells, respectively. Scale bars: 50 μm. See also Supplementary Figs. 9, 10 and Supplementary Data 3.

all downregulated (Supplementary Fig. 11d). This result, plus the fact that the expression of *NidaLMI1* in STs[36] was earlier than the expression of other ST genes, i.e., *NidaMYB5-2*, *NidaGL3*, *NidaTT8*, and *NidaGL2*, indicate that *NidaLMI1* may function as an upstream activator of the hypothetical MBW complex-*GL2* module for STs (Supplementary Fig. 11e).

https://doi.org/10.1038/s41467-025-64028-3

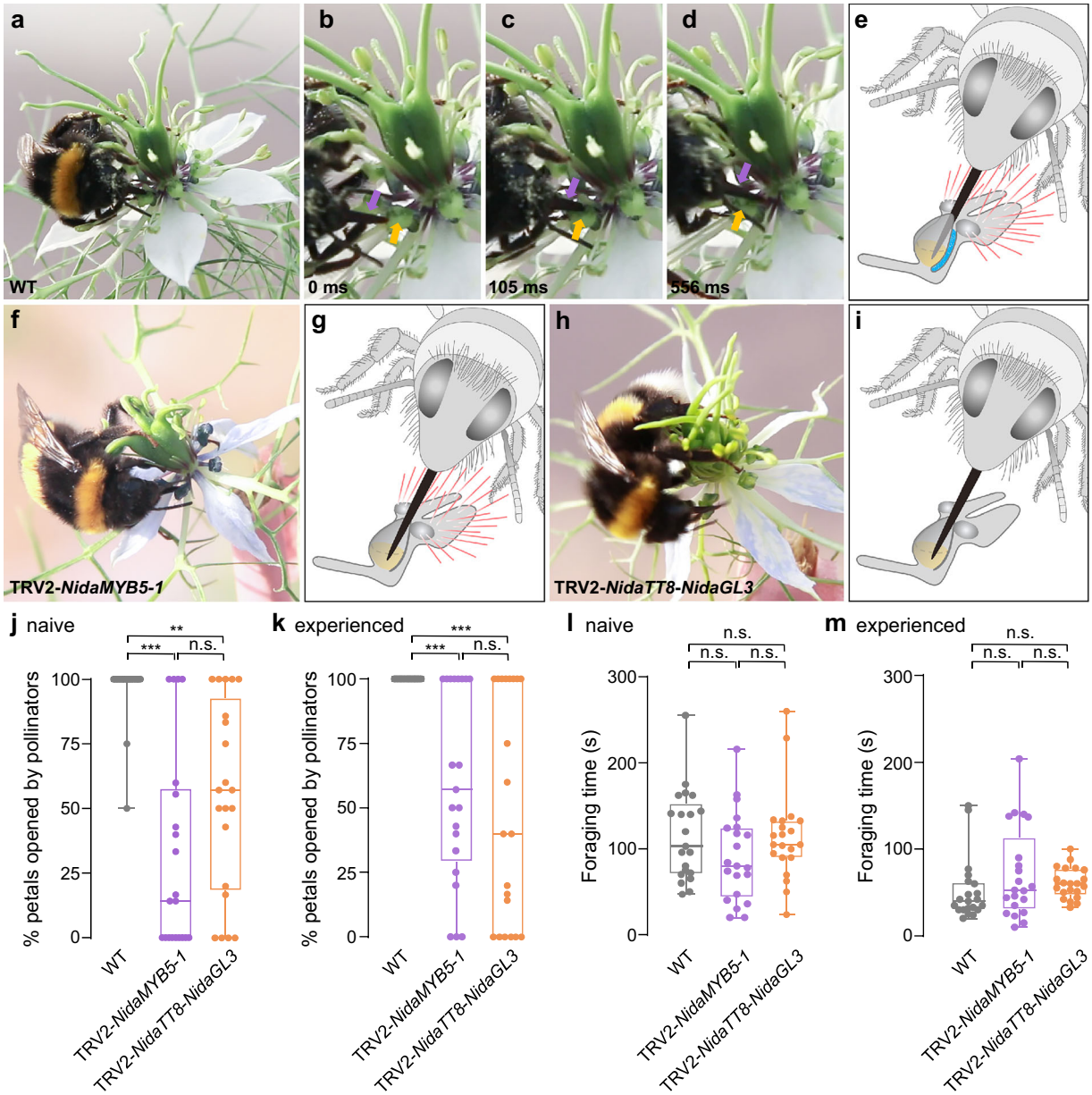


**Fig. 5 | Ecological functions of short trichomes and long hairs in *Nigella damascena*.** **a**–**i** The visiting behaviors of bumblebees on wild-type (**a**–**e**, petals with short trichomes and long hairs), TRV2-*NidaMYB5-1*- (**f, g**, petals with only long hairs) and TRV2-*NidaTT8-NidaGL3*- (**h, i**, petals lacking both short trichomes and long hairs) treated flowers. Movie frames showing the moments before (**b**), during (**c**), and after (**d**) the bumblebee foraged for nectar in a petal. The yellow arrow indicates the entrance to the petal nectary. The purple arrow indicates the proboscis of the bumblebee. Illustrations showing the accessibility of bumblebees to nectar in different petals (**e, g, i**). ms: millisecond. See Supplementary Movies 1–3 for details. **j, k** Percentages of petals opened by naive (**j**) and experienced (**k**) bumblebees in wild-type and VIGS-treated flowers. **l, m** Foraging times of naive (**l**) and experienced (**m**) bumblebees on wild-type and VIGS-treated flowers. In (**j**–**m**), the box is bounded by the first and third quartiles with a horizontal line at the median, and whiskers extend to the minimum and maximum values. $^{**}P < 0.01$, $^{***}P < 0.001$, n.s., not significant (Kruskal-Wallis test). Each experimental group comprised 21 independent replicates, each involving one bumblebee and one flower. Source data for (**j**–**m**) are provided in Supplementary Data 4.

## Ecological functions of STs and LHs in *N. damascena*

It is noteworthy that knocking down most of the candidate genes produced glabrous petals or those with only LHs, thus providing us an excellent opportunity to explore the potential ecological functions of STs and LHs. By using bumblebees (*Bombus terrestris*), one of the legitimate pollinators[35,39], we conducted pollination studies on wild-type flowers (with STs and LHs), TRV2-*NidaMYB5-1*-treated flowers (with only LHs, but without STs), and TRV2-*NidaTT8-NidaGL3*-treated flowers (lacking both STs and LHs) (Fig. 5 and Supplementary Data 4). We found that 90% of naive bumblebees and 100% of experienced ones successfully opened the lips of all the petals in wild-type flowers and reached nectar (Fig. 5a–e, j, k and Supplementary Movie 1). In contrast, when naive and experienced bumblebees visited TRV2-*NidaMYB5-1*- and TRV2-*NidaTT8-NidaGL3*-treated flowers, they failed to open petal lips in most cases, with no significant differences observed between the two types of VIGS-treated flowers (Fig. 5f–k and Supplementary Movies 2, 3). This occurred because the gap between the upper and lower lips, naturally present in wild-type petals, was closed in the VIGS-treated petals due to the absence of STs (Supplementary Fig. 9e–g). In addition, when comparing the foraging time of the bumblebees, we did not find significant differences among different types of flowers regardless of whether naive or experienced

pollinators were used (Fig. 5l, m). These results indicate that the presence of STs may serve as tiny pillars to prop open upper and lower lips, hence facilitating the access of pollinators to nectar, whereas the role of LHs in bumblebee pollination is negligible.

### Evolution of STs and LHs and their underlying mechanisms

To understand how STs and LHs have evolved in *Nigella*, we carefully observed the cellular features and developmental processes of hairs on petals of *N. integrifolia*, which are unicellular, with a wide distribution and relatively uniform lengths (Fig. 6a–c and Supplementary Fig. 12a, b). For the convenience of comparison with *N. damascena*, we divided the hairs into two types, i.e., Type 1 hairs (T1Hs) and Type 2 hairs (T2Hs), with T2Hs specifically referring to hairs positionally corresponding to STs on petals of *N. damascena*, and T1Hs representing hairs in other regions. When comparing T1Hs on the adaxial side of the lower lip (positionally corresponding to LHs on *N. damascena* petals) with T2Hs, we found that T2Hs (median number: 211; median length: 261.74 μm) are denser but slightly shorter than T1Hs (median number: 129; median length: 289.60 μm) (Fig. 6d, e and Supplementary Data 5). Nuclear size and ploidy level comparison revealed that the nuclei of T1Hs and T2Hs were approximately twice as big as the PC nuclei (Fig. 6f–i and Supplementary Fig. 12c, d) and had a higher ploidy level of 4C than the dominant 2C cells (Supplementary Fig. 12e–g), suggestive of the occurrence of one round of endoreduplication in the hair cells. By tracing the development of T1Hs and T2Hs, we found that T1Hs initiate continuously from S6 to S9, and reach their final lengths by S12, while T2Hs initiate at S10 and continue elongating until S12 (Fig. 6j, Supplementary Fig. 12h and Supplementary Data 5). A comparison of these results with those in *N. damascena* indicates that the evolution of obviously different STs and LHs was likely caused by the elongation of T1Hs on the adaxial side of the lower lip, but the shortening of T2Hs on the contact surfaces between upper and lower lips.

To gain some insights into the molecular mechanisms underlying the evolution of STs and LHs in *Nigella*, we retrieved putative orthologs of genes that play critical roles in LHs and/or STs of *N. damascena* petals (i.e., *MYB5-1*, *MYB5-2*, *GL3*, *TT8*, *GL2*, and *LMI1*) from the reference transcriptome of *N. integrifolia*[40]. Phylogenetic analyses revealed that while *MYB5-1* and *MYB5-2* were duplicated before the divergence of the Ranunculaceae, all examined genes were single-copied in *Nigella* species (Supplementary Fig. 13). DGE profiling of *N. integrifolia* petals across eight developmental stages comparable to *N. damascena* revealed that while all examined genes were expressed at varying levels throughout petal development, they showed expression peaks at S8/9 (Fig. 6k and Supplementary Data 6). mRNA in situ hybridization results further showed that *NiinMYB5-1* and *NiinGL3* were expressed in regions containing emerging hair cells; *NiinGL2* was specifically expressed in hair cells; *NiinLMI1* was only expressed inside the nectary chamber and the surrounding region where T2Hs would arise; *NiinMYB5-2* and *NiinTT8*, however, were not expressed in petal hairs (Fig. 6l–p and Supplementary Fig. 14). These results suggest that in *N. integrifolia*, *NiinMYB5-1*, *NiinGL3*, and *NiinGL2* are all required for the formation of petal hairs, and *NiinLMI1* is only involved in the initiation of T2Hs. Interestingly, when comparing the programs for petal trichomes/hairs between *N. integrifolia* and *N. damascena*, we found that *MYB5-1*, *GL3*, *GL2*, and *LMI1* showed similar expression patterns and possibly conserved functions, but *MYB5-2* was specific for LHs, and *TT8* was specific for STs (Fig. 7a, b). These findings suggest that independent recruitment of *TT8* and *MYB5-2* into the trichome specification program, followed by refining of their expression patterns, may be the key to the evolution of STs and LHs in *Nigella* (Fig. 7c, d).

## Discussion

In this study, by applying multiple strategies, we for the first time provided a comprehensive understanding of differences and relationships among different types of protrusive cells on petals. We found that: (1) while the CCs, STs, and LHs on *N. damascena* petals are all unicellular, they differ not only in shape, length, number, distribution pattern, surface ornamentation, relative nuclear size, and possibly ploidy level, but also in developmental process and molecular basis; (2) *NidaMIXTA* is involved in CC development, but not in the formation of STs and LHs; (3) the identities of STs and LHs are specified by different combinations of genes encoding components in the hypothetical MBW complex-*GL2* module; (4) in contrast to LHs, which are dispensable for the visit of bumblebees, STs serve as tiny pillars to prop open the petal lips and facilitate the access of pollinators to nectar; and (5) STs and LHs may have evolved from LH-like ancestors in *Nigella* through independent co-option of *TT8* and *MYB5-2*, respectively. These results provide new insights into the developmental and evolutionary mechanisms and the adaptive significance of protrusive cells.

### CCs, STs, and LHs: differences and relationships

Early studies have proposed that petal trichomes and CCs are closely related and that the relative timing of *MIXTA* expression may determine their final fates[20–23], but direct evidence is still lacking. In this study, we revealed that, on petals of *N. damascena*, while the CCs and the two types of trichomes (i.e., STs and LHs) are unicellular, they are apparently different at multiple levels. First, they differ in cellular features, including shape, length, number, cuticular ornamentation, relative nuclear size, and possibly ploidy level. Second, they experience distinct developmental trajectories, with LHs starting to emerge from S6, but STs from S10, and CCs from S11. Last but not least, while the CC identity gene in *N. damascena* remains to be identified, CCs and STs/LHs are specified by totally different genetic programs. We found that *NidaMIXTA*, a homolog of the well-known CC/trichome identity gene, is involved in the cuticle development of CCs, but does not affect STs and LHs. In contrast, LHs and STs are specified by related programs, with *NidaMYB5-1*, *NidaMYB5-2*, *NidaGL3*, and *NidaGL2* for LHs, whereas *NidaLMI1*, *NidaMYB5-1*, *NidaGL3*, *NidaTT8*, and *NidaGL2* for STs. By taking the expression patterns and functions of all trichome identity genes into account, we propose that the common regulators *NidaMYB5-1*, *NidaGL3*, and *NidaGL2* constitute the core of the program, defining the trichome identity of a cell. The developmental fates of STs and LHs mainly depend on the expression timing of the core regulators and the spatial expression of ST- or LH-specific genes.

Interestingly, when we compared the trichome identity networks in *N. damascena* with those identified in other species, we found two special aspects. One concerns the contribution of MYB family genes to trichome specification. In *N. damascena*, *NidaMYB5*s, rather than the homologs of known trichome identity genes *MIXTA* and *GL1*, are involved in the specification of STs and LHs. However, *MYB5*-like genes are usually involved in flavonoid accumulation[41–44], or occasionally participate in trichome development, as reported in *A. thaliana* and *G. hirsutum*[45,46]. The other peculiarity is related to the mechanisms underlying the fate determination of different types of trichomes on one organ. Available data have shown that functional divergence of duplicate genes (e.g., *MIXTA* duplicate copies in *G. hirsutum*) [8,9,47] and differential regulation of certain genes (e.g., *Woolly* [*Wo*] and *GLAND CELL REPRESSOR*s [*GCR*s] in *S. lycopersicum*) [48,49] play critical roles. Yet, our findings revealed a different mechanism in *N. damascena*. We showed that the component differences in the potential MBW complex underlie the divergence of STs and LHs, with LHs requiring two MYB genes (*NidaMYB5-1* and *NidaMYB5-2*) and one bHLH gene (*NidaGL3*), but STs relying on one MYB gene (*NidaMYB5-1*) and two bHLH genes (*NidaTT8* and *NidaGL3*). These findings expand our knowledge of the conservativeness and flexibility of the trichome specification programs across angiosperms.

### Evolutionary mechanisms of STs and LHs in *Nigella*

The evolution of trichomes on *Nigella* petals involves the concurrent origination of STs and LHs and the formation of their spatial patterns (Fig. 7c). In this study, by comparing the copy number and expression

https://doi.org/10.1038/s41467-025-64028-3

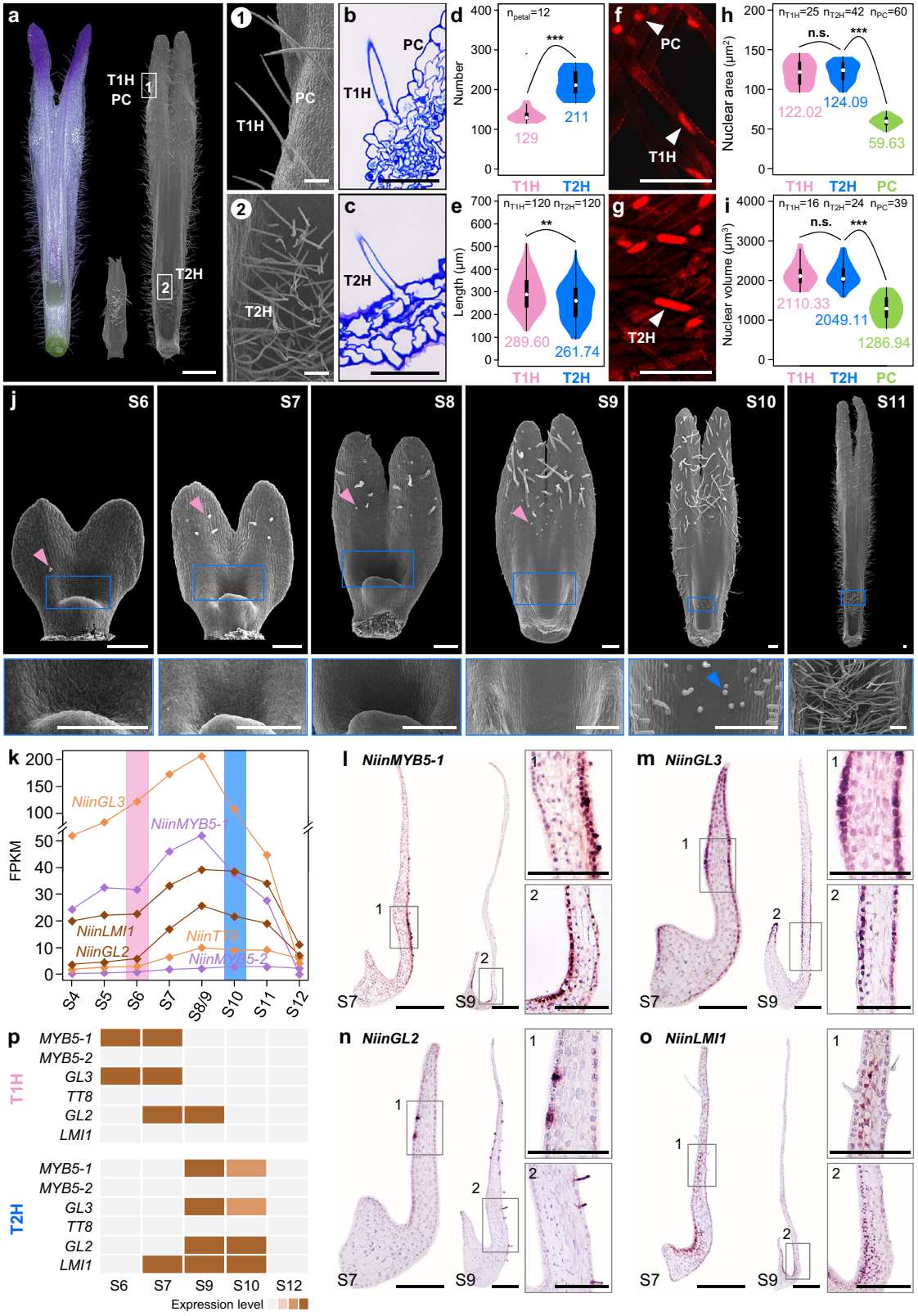


patterns of the six key trichome genes between *N. damascena* and *N. integrifolia*, we found that all the investigated genes remained single-copied and that the orthologs of all but two (i.e., *TT8* and *MYB5-2*) showed similar expression patterns. In *N. damascena*, *NidaTT8* and *NidaMYB5-2* play essential roles in the formation of STs and LHs on petals, respectively, but in *N. integrifolia*, neither *NiinTT8* nor *NiinMYB5-2* was expressed in petal hairs. Notably, *TT8*-like genes have an ancient origin traceable to the most recent common ancestor (MRCA) of seed plants[50], while *MYB5*-like genes originated later and can be traced back to the MRCA of angiosperms[51]. Moreover, the general functions of both *TT8*- and *MYB5*-like genes in angiosperms are associated with flavonoid biosynthesis[41–43,52–54], with a few exceptions in *A. thaliana* and *G. hirsutum*[45,46,55]. Presumably, the independent co-option of two evolutionarily conserved pigment regulatory genes (i.e., *TT8*

**Fig. 6 | Cellular features and developmental processes of hairs and expression patterns of key candidate genes in *Nigella integrifolia* petals. a** The distribution of Type 1 hairs (T1Hs), Type 2 hairs (T2Hs), and pavement cells (PCs) on a mature petal under stereomicroscope and scanning electron microscope. Numbered regions (1–2) are magnified to show T1Hs/PCs and T2Hs, respectively. **b, c** Semi-thin sections of regions containing T1Hs/PCs (**b**) and T2Hs (**c**). **d** Total numbers of T1Hs and T2Hs on each petal. **e** Lengths of T1Hs and T2Hs. **f, g** Propidium iodide (PI) staining of T1Hs/PCs (**f**) and T2Hs (**g**). The white arrowhead points to the nucleus. **h** The largest PI fluorescence areas in T1Hs, T2Hs, and PCs. **i** Volumes of reconstructed three-dimensional nuclei in T1Hs, T2Hs, and PCs. In (**d, e, h**) and (**i**), violin outline width shows the density of the data; the thick bar represents the interquartile range (IQR) between the first and third quartiles, with the median marked by a white dot and labeled with the corresponding value; whiskers extend up to 1.5 times the IQR. $^{**}P < 0.01$, $^{***}P < 0.001$, n.s., not significant (two-sided Mann-Whitney *U* test). Source data are provided in Supplementary Data 5. **j** The development of T1Hs and T2Hs. The images below petals show the magnified views of the boxed regions containing T2Hs (dark blue). Pink and dark blue arrowheads point to the emerging T1H and T2H, respectively. For each stage, at least 3 petals were observed. **k** Expression profiles of key candidate genes across eight developmental stages of petals. Pink and dark blue bars indicate the stages when T1Hs and T2Hs arise, respectively. Source data are provided in Supplementary Data 6. **l**–**o** Results of mRNA in situ hybridization for *NiinMYB5-1* (**l**), *NiinGL3* (**m**), *NiinGL2* (**n**), and *NiinLMI1* (**o**) in *N. integrifolia* petals at different stages. All results are representative of at least two independently repeated experiments. See also Supplementary Fig. 14. Scale bars: (**a** left) 1 mm; (**a** right, **b**, **c**, **f**, **g**) 50 μm; (**j**, **l**–**o**) 100 μm. **p** A summary of gene expression patterns throughout petal development of *N. integrifolia*. The expression levels are determined based on the FPKM values and the intensities of in situ hybridization signals (the darker, the higher).

and *MYB5-2*) into the existing trichome specification program led to the origination of STs and LHs on petals in *Nigella*.

Ancestral character-state reconstruction indicated that the loss of hairs on the abaxial side of lower lip lobes was the key to the spatial patterning of STs and LHs on *Nigella* petals (Fig. 7c). Despite lacking direct evidence, a study in *A. thaliana* has shown that the abaxial polarity factor *KANADI1* (*KAN1*) represses the trichome initiation on the abaxial side of leaves during the juvenile stage[56]. It is plausible that a similar mechanism may have evolved during the trichome evolution of *Nigella*. In addition, based on current and previous studies, we propose that the recruitment of *LMI1* into the trichome specification program in the MRCA of *Nigella* may be responsible for the positioning of STs, for four reasons. First, as revealed in *N. damascena* and *N. integrifolia*, the *LMI1* genes were specifically expressed surrounding the nectary chamber, overlapping with the region where STs are located[36]. Second, *NidaLMI1* has been reported to be critical for the formation of STs; knockdown of it resulted in the loss of STs[36]. Third, *NidaLMI1* may function as an upstream regulator of the trichome identity genes in *N. damascena* (Supplementary Fig. 11). Fourth, and most importantly, in *Delphinium anthriscifolium* (Delphinieae), a species close to *Nigella*, the *LMI1* ortholog was found to regulate the differential growth between the adaxial and abaxial sides of lateral petals, rather than the development of trichomes[57]. We propose that the *LMI1* genes pre-pattern the localization of trichomes around the nectary chamber in *Nigella*, providing a positional signal. Further studies to explore how *TT8* and *MYB5-2* were recruited, and how the regulatory links between the trichome identity program and potential positioning factors (e.g., abaxial polarity genes and *LMI1*) were established, will provide deeper insights into petal trichome evolution and pattern formation in *Nigella*.

### Adaptive significance of STs and LHs on *Nigella* petals

Several scenarios have been proposed regarding the possible functions of STs on *Nigella* petals: filtering pollen, reducing nectar evaporation, and preventing unfavorable visitors[32,33]. Notably, the prerequisite of these hypotheses is that the gap between the upper and lower lips remains in the absence of STs. However, in this study, we unexpectedly found that the absence of STs caused the closing of petal lips. As a result, most naive and experienced bumblebees failed to open the lips and reach nectar when visiting flowers without STs on petals. Our findings neither support nor reject the previous hypotheses, but instead provide direct experimental evidence that STs act as tiny pillars in maintaining petal lip opening and facilitate the access of suitable pollinators to nectar. Notably, the function of trichomes in regulating the structures of flowers or floral organs has been reported in other species, usually as "linkers"[8,58,59]. For instance, in *G. hirsutum*, trichomes on the petal blade link adjacent petals together through a mechanical entanglement[8]. In cultivated tomato, the interlocking trichomes at anther margins can unite neighboring stamens to generate a closed anther cone and cleistogamy[58]. Interestingly, trichomes that function as linkers are generally soft, relatively dispersed, and closely intertwined. In contrast, STs that act as pillars on *Nigella* petals are rigid, densely arranged, and barely intertwined. These findings imply that the functions of trichomes in regulating the structures of flowers and floral organs are dependent on their cellular features.

Notably, while the current study revealed a negligible role of LHs in bumblebee pollination, we cannot rule out the potential functions of LHs for other effective pollinators. It has been shown that when honey bees (*Apis mellifera*) landed on wild-type flowers of *N. damascena* trying to gather nectar from petals, they retracted their forelegs and gripped petal lobes with middle legs[35], indicating that LHs could potentially provide grip for honey bees. Besides, in *N. damascena* and *N. orientalis*, LHs are shiny and reflective under ultraviolet light like pseudonectaries and are mainly distributed on the distal part of the petal[35,37]. Therefore, they may offer visual signals to pollinators, similar to the function of trichomes on tepal tips of *Narcissus tazetta*[60]. Of course, there are other possibilities. LHs might be able to offer tactile signals to stimulate pollinators for further exploration. An interesting example from the deceptive orchid, *Ophrys fusca,* showed that trichomes on the labellum mimic hairs of female insects, which provide male pollinators with real tactile senses for pseudocopulation[61]. Alternatively, since most wild *Nigella* species blossom during hot, dry seasons, LHs may reduce evaporation and maintain moisture on the petal epidermis, helping plants adapt to arid environments, similar to the hairs protecting sunken stomata in desert plants[62].

## Methods

### Plant materials and growth conditions

Seeds of *N. damascena* and *N. integrifolia* were purchased from B & T World Seeds (Paguignan, France). They were sown in a 2:1 mixture of vermiculite and nutrient soil and grown at 24 °C, 60% relative humidity, and a 12-h-light/12-h-dark photoperiod. The voucher specimens of *N. damascena* and *N. integrifolia* have been deposited in the Chinese National Herbarium (PE), Institute of Botany, Chinese Academy of Sciences, under accession numbers 02604841 and 02604842.

### Microscopy and histology

The stereomicroscope images of mature petals were obtained by using a Leica DVM6 digital microscope. For scanning electron microscopy (SEM), the samples were fixed in FAA, containing 3.7% (v/v) formaldehyde, 5% (v/v) acetic acid, and 50% (v/v) ethanol, at 4 °C overnight, and then dehydrated in a gradient water-ethanol series. After being critical-point dried by $CO_2$ and sputter-coated by gold, the samples were observed under a Hitachi S-4800 field emission scanning electron microscope. For histological observations, mature petals were fixed in 4% (w/v) paraformaldehyde (pH 7.2) at 4 °C overnight and embedded in SPI-PON 812 resin. Semi-thin sections (1.5 μm) were prepared on a Leica EM UC7 ultramicrotome, stained with 0.33% (w/v) toluidine blue for 30 s and imaged under a Leica DM5000B microscope equipped with a Leica DFC450 C camera.

https://doi.org/10.1038/s41467-025-64028-3

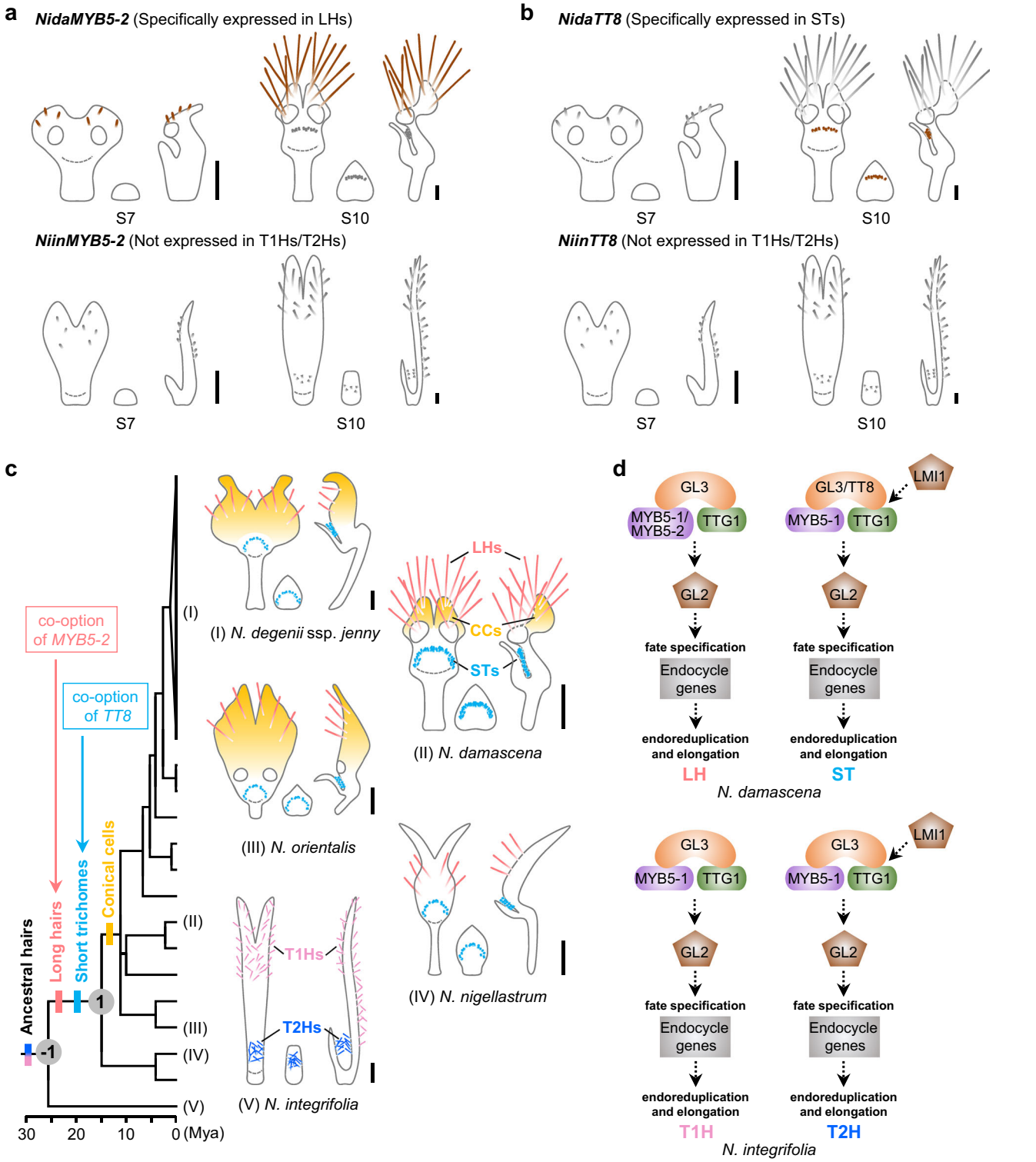


**Fig. 7 | Possible evolutionary scenarios for the evolution of short trichomes and long hairs on *Nigella* petals. a, b** Schematic diagrams showing expression patterns of *MYB5-2* (**a**) and *TT8* (**b**) in S7 and S10 petals of *Nigella damascena* and *N. integrifolia*. The expression signals are marked by brown shadings. Scale bars: 200 μm. **c** Evolutionary history of petal hairs/trichomes in *Nigella*. The simplified phylogenetic tree and divergence times were adopted from a previous study[32]. Schematic diagrams (I)–(V) show petals of five representative *Nigella* species. From nodes -1 to 1, independent co-option of *TT8* and *MYB5-2* has resulted in the origination of STs and LHs, respectively. Scale bars: 1 mm. **d** Molecular mechanisms underlying the formation of trichomes/hairs on *Nigella* petals. Top: a refined functional model for the formation of LHs and STs on petals of *N. damascena*. Bottom: a deduced model for the formation of T1Hs and T2Hs on petals of *N. integrifolia*. The interactions among proteins of genes of interest are illustrated in reference to *Arabidopsis thaliana*. LHs, long hairs; STs, short trichomes; T1Hs, Type 1 hairs; T2Hs, Type 2 hairs.

### Nuclear size measurement and ploidy level determination

To measure nuclear sizes of different types of cells on petals, mature petals of *N. damascena* and *N. integrifolia* were fixed in FAA at 4 °C overnight and immersed in $ddH_2O$ containing 100 μg $mL^{-1}$ PI or 5 μg $mL^{-1}$ DAPI for 10 min, and rinsed in $ddH_2O$ for three times. Stained samples were imaged under a Zeiss LSM 980 Elyra 7 confocal laser scanning microscope. PI was excited by a 488 nm diode laser and detected in a 617 nm emission spectrum. DAPI was excited by a 405 nm diode laser and detected in a 465 nm emission spectrum. Optical sections were reconstructed in ZEN 2012. The largest PI fluorescence areas of nuclei were measured in ImageJ. The volumes of reconstructed three-dimensional nuclei were measured using MorphoGraphX as follows[63]. First, the "Stack/Filters/Gaussian Blur Stack (x, y, z sigma = 0.7)" process was applied. Second, edge detection was performed using "Stack/Morphology/Edge Detect (threshold 10,000)". The resulting stack was then manually corrected with the Pixel Editor tool to remove noise and misrepresented nuclei. The mesh surface was generated via "Marching Cubes Surface (cube size = 1)" followed by smoothing and subdividing the mesh. Each nucleus was individually seeded, and watershed segmentation was executed. Finally, nuclear volumes were calculated using "Heat Map (Heat Map type: volume; signal average; global coordinates)".

To determine the ploidy levels of cells in petals of *N. damascena* and *N. integrifolia*, we conducted flow cytometry analysis. Petals were dissected under a stereomicroscope, and only regions covering STs or LHs in *N. damascena* or T1Hs or T2Hs in *N. integrifolia* were collected. Samples were chopped with a razor blade in 0.5 mL nuclei isolation buffer containing 30 mM sodium citrate, 45 mM $MgCl_2$, 20 mM MOPS, 20 mM NaCl, 20 mM EDTA $Na_2{\cdot}2H_2O$, 0.1% (v/v) Triton X-100, 0.5% (v/v) Tween-20, and 2% PVPK12 (pH 7.0)[64]. The nuclei were filtered through a 48-μm filter and stained with 5 μg $mL^{-1}$ DAPI. Nuclear DNA content was analyzed with an LSR Fortessa flow cytometer (BD Biosciences), and then analyzed with FlowJo software. Data were collected for approximately 10,000 nuclei per sample and presented on a linear axis.

### Digital gene expression profiling

Reference transcriptomes of *N. damascena* and *N. integrifolia* as well as DGE profiles and gene co-expression modules across eight petal stages of *N. damascena* were retrieved from previous studies[36,40]. DGE profiles for the four parts of S10 petals of *N. damascena* (each with four biological replicates) and those for petals at eight stages of *N. integrifolia* (each with three biological replicates) were generated in this study. The developmental stages of petals were defined according to a previous study[32]. For each sample, the total RNA was extracted using the SV Total RNA Isolation System (Promega) and a library was constructed and sequenced on Illumina HiSeq2000 (Novogene) for generating paired-end reads of 150 bp. Clean reads were mapped to the corresponding reference transcriptome, and fragments per kilobase per million mapped reads (FPKM) values were calculated by RSEM[65]. The average FPKM value of replicates was used as the gene expression level in the corresponding sample. Genes having FPKM ≥ 1.0 were defined as expressed.

### mRNA in situ hybridization

Total RNAs were extracted from floral buds of *N. damascena* and *N. integrifolia*, respectively, as described above and reverse-transcribed using SuperScript III First-Strand Synthesis System (Life Technologies). cDNA fragments of candidate genes were amplified and cloned into the p*EASY*-Blunt Zero cloning vector (TransGen) for sequencing. Gene-specific fragments were then amplified and used as templates for synthesizing antisense and sense digoxigenin-labeled RNA probes using a DIG RNA labeling kit (Roche). For mRNA in situ hybridization, petals or floral buds of *N. damascena* and *N. integrifolia* at different developmental stages were immersed in fresh 4% (w/v) paraformaldehyde (pH 7.2) and embedded in Paraplast (Sigma). Serial sections (8 μm) were prepared and mounted on slides, which were then placed on a slide warmer at 42 °C overnight. After dewaxing, rehydration, and dehydration, the sections were hybridized with RNA probes at 55 °C overnight. After hybridization, the slides were washed in saline sodium citrate (SSC) and incubated with an anti-digoxigenin-AP antibody (Roche) for 2 h at room temperature. The hybridization signals were detected by NBT/BCIP (Roche) color reaction at room temperature overnight in the dark. Images were captured under a Leica DM5000 B microscope equipped with a Leica DFC450 C camera. Primers used for cDNA amplification and probe preparation are provided in Supplementary Data 7; relative positions of the probes to their cDNA sequences are shown in Supplementary Figs. 4, 6, 7, 9, 10, and 14.

### Virus induced gene silencing

Fragments used for VIGS overlapped with those used for in situ hybridization (Supplementary Data 3, Supplementary Figs. 4, 6, 7, 9 and 10), which were introduced into the tobacco rattle virus (TRV2)-based pYL156 vector and transformed into *Agrobacterium tumefaciens* strain GV3101. The strains carrying either TRV1 or TRV2 (containing the target fragment) were cultured separately in LB culture medium (50 μg $mL^{-1}$ Kanamycin, 50 μg $mL^{-1}$ Gentamycin, and 25 μg $mL^{-1}$ Rifampicin) overnight in a 28 °C shaker at 220 rpm. Bacteria were harvested by centrifugation at 4000×*g* for 15 min and resuspended in MMA buffer (10 mM $MgCl_2$, 10 mM MES, and 200 μM acetosyringone) till the optical density ($OD_{600}$) of approximately 2.0. Seedlings at the 5–7 true leaf stage were rinsed and immersed in a 1:1 (v/v) mixture of TRV1 and TRV2 bacterial suspensions. After vacuum infiltration for 2 min, the seedlings were transplanted and completely covered with black plastic for 48 h. They were then grown under a 12-h-light/12-h-dark photoperiod until flowering. As a negative control (mock), parallel infiltrations were performed using a 1:1 (v/v) mixture of TRV1 and the empty TRV2 strains. The morphology and micromorphology of petals with potential phenotypic changes were investigated under a stereomicroscope and SEM as described above. To evaluate the silencing efficiency of the candidate gene(s) and the regulatory relationships among interested genes, gene expression levels in VIGS-treated petals were determined by quantitative reverse transcription-polymerase chain reaction (qRT-PCR). Petals at stage 10 were collected from wild-type, mock, and VIGS-treated plants. For each VIGS treatment, two or three biological replicates were included. All reactions were performed with three technical replicates. The housekeeping gene *NidaACTIN* was used as an internal quantitative control. The relative expression values were calculated using the comparative CT ($2^{-\Delta\Delta CT}$) method. Primers used for vector construction and qRT-PCR are listed in Supplementary Data 7.

### Pollination studies

Bumblebee colonies were purchased from Biobest company (Shandong, China) and maintained in a greenhouse at 25 °C. They were fed on a provided sugar solution at all times, supplemented with pollen every two days. On the day before the pollination study, the bumblebees were separated into different plastic jars, fed with 350 μL 20% (w/v) sucrose solution and isolated overnight in the dark. Of the bumblebees used, the naive ones were those that had never visited flowers of *N. damascena*, whereas the experienced ones were those that had been trained with wild-type flowers and were capable of opening petal lips. Pollination assays were set in a greenhouse under sunny conditions (25 °C) and performed in a flight cage with the following dimensions: 180 cm (length) × 80 cm (width) × 120 cm (height). For each observation, only one bumblebee was released into the flight cage, where only one plant with a flower at 1 day post-anthesis was displayed. During each foraging bout, i.e., the interval between landing on and leaving a flower, the number of petals with their lips opened and unopened by the bumblebee and the foraging time were recorded

(Supplementary Data 4). To avoid repeated use, all experimental bumblebees were marked before returning to the hive.

### Phylogenetic analysis

Sequences of *MYB5-1*, *MYB5-2*, *GL3*, *TT8*, *GL2*, and *LMI1* of *N. damascena* and *N. integrifolia* were obtained from the reference transcriptomes. Their homologs from other species were retrieved from publicly available databases by BLAST searches (Supplementary Data 8). For each gene lineage, protein sequences were aligned with Clustal X 2.0.6[66] and manually adjusted using MEGA X[67]. Phylogenetic analyses were performed on matrices containing only alignable coding sequences in IQ-TREE 1.6.10[68] using the maximum-likelihood method. Analysis was carried out using 10,000 bootstrap replicates. Trees were rooted with genes from *Amborella trichopoda*.

### Statistics and reproducibility

In general, the two-sided Mann-Whitney *U* test was used to assess significant differences between two samples, while the Kruskal-Wallis test was used in pollination studies, and the unpaired two-tailed Student's *t* test was used in qRT-PCR assays. Numbers of samples and repetitions for each experiment were indicated in the figure legends and methods.

### Reporting summary

Further information on research design is available in the Nature Portfolio Reporting Summary linked to this article.

## Data availability

The RNA-seq data have been deposited in the NCBI Short Read Archive with accession numbers PRJNA1267719 and PRJNA1274143. All other data supporting the findings of this study are available in the paper and Supplementary Information files. Source data are provided with this paper.

## References


1. Kay, Q., Daoud, H. & Stirton, C. Pigment distribution, light reflection and cell structure in petals. *Bot. J. Linn. Soc.* **83**, 57–83 (1981).
2. Whitney, H. M. et al. Why do so many petals have conical epidermal cells? *Ann. Bot.* **108**, 609–616 (2011).
3. Cavallini-Speisser, Q., Morel, P. & Monniaux, M. Petal cellular identities. *Front. Plant Sci.* **12**, 745507 (2021).
4. Endress, P. K. & Matthews, M. L. Elaborate petals and staminodes in eudicots: diversity, function, and evolution. *Org. Divers. Evol.* **6**, 257–293 (2006).
5. Fu, X. et al. Petal development and elaboration. *J. Exp. Bot.* **73**, 3308–3318 (2022).
6. Bradshaw, E. et al. Comparative labellum micromorphology of the sexually deceptive temperate orchid genus *Ophrys*: diverse epidermal cell types and multiple origins of structural colour. *Bot. J. Linn. Soc.* **162**, 504–540 (2010).
7. Oelschlägel, B., Gorb, S., Wanke, S. & Neinhuis, C. Structure and biomechanics of trapping flower trichomes and their role in the pollination biology of *Aristolochia* plants (Aristolochiaceae). *New Phytol.* **184**, 988–1002 (2009).
8. Tan, J., Walford, S. A., Dennis, E. S. & Llewellyn, D. Trichomes control flower bud shape by linking together young petals. *Nat. Plants* **2**, 16093 (2016).
9. Tan, J., Walford, S. A., Dennis, E. S. & Llewellyn, D. J. Trichomes at the base of the petal are regulated by the same transcription factors as cotton seed fibers. *Plant Cell Physiol.* **61**, 1590–1599 (2020).
10. Ren, H. et al. Spatio-temporal orientation of microtubules controls conical cell shape in *Arabidopsis thaliana* petals. *PLoS Genet.* **13**, e1006851 (2017).
11. Saffer, A. M., Carpita, N. C. & Irish, V. F. Rhamnose-containing cell wall polymers suppress helical plant growth independently of microtubule orientation. *Curr. Biol.* **27**, 2248–2259 (2017).
12. Li, S. et al. An ancient RAB5 governs the formation of additional vacuoles and cell shape in petunia petals. *Cell Rep.* **36**, 109749 (2021).
13. Ren, H. et al. PP2A interacts with KATANIN to promote microtubule organization and conical cell morphogenesis. *J. Integr. Plant Biol.* **64**, 1514–1530 (2022).
14. Noda, K. I., Glover, B. J., Linstead, P. & Martin, C. Flower colour intensity depends on specialized cell shape controlled by a Myb-related transcription factor. *Nature* **369**, 661–664 (1994).
15. Baumann, K. et al. Control of cell and petal morphogenesis by R2R3 MYB transcription factors. *Development* **134**, 1691–1701 (2007).
16. Zahid, S., Schulfer, A. F. & Di Stilio, V. S. A eudicot *MIXTA* family ancestor likely functioned in both conical cells and trichomes. *Front. Plant Sci.* **14**, 1288961 (2023).
17. Di Stilio, V. S., Martin, C., Schulfer, A. F. & Connelly, C. F. An ortholog of *MIXTA-like2* controls epidermal cell shape in flowers of *Thalictrum*. *New Phytol.* **183**, 718–728 (2009).
18. Oshima, Y. et al. MIXTA-like transcription factors and WAX INDUCER1/SHINE1 coordinately regulate cuticle development in *Arabidopsis* and *Torenia fournieri*. *Plant Cell* **25**, 1609–1624 (2013).
19. Lu, H. C. et al. R2R3-MYB genes coordinate conical cell development and cuticular wax biosynthesis in *Phalaenopsis aphrodite*. *Plant Physiol.* **188**, 318–331 (2022).
20. Esau, K. *Plant Anatomy*. (John Wiley and Sons, 1953).
21. Martin, C. & Paz-Ares, J. MYB transcription factors in plants. *Trends Genet.* **13**, 67–73 (1997).
22. Glover, B. J. & Martin, C. Specification of epidermal cell morphology. *Adv. Bot. Res.* **31**, 193–217 (2000).
23. Glover, B. J., Perez-Rodriguez, M. & Martin, C. Development of several epidermal cell types can be specified by the same MYB-related plant transcription factor. *Development* **125**, 3497–3508 (1998).
24. Martin, C. et al. The mechanics of cell fate determination in petals. *Philos. Trans. R. Soc. Lond. B. Biol. Sci.* **357**, 809–813 (2002).
25. Dong, Y. et al. Advances in understanding epigenetic regulation of plant trichome development: a comprehensive review. *Hortic. Res.* **10**, uhad145 (2023).
26. Yang, C. & Ye, Z. Trichomes as models for studying plant cell differentiation. *Cell. Mol. Life Sci.* **70**, 1937–1948 (2013).
27. Oppenheimer, D. G., Herman, P. L., Sivakumaran, S., Esch, J. & Marks, M. D. A *myb* gene required for leaf trichome differentiation in Arabidopsis is expressed in stipules. *Cell* **67**, 483–493 (1991).
28. Rerie, W. G., Feldmann, K. A. & Marks, M. D. The *GLABRA2* gene encodes a homeo domain protein required for normal trichome development in *Arabidopsis*. *Genes Dev.* **8**, 1388–1399 (1994).
29. Walker, A. R. et al. The *TRANSPARENT TESTA GLABRA1* locus, which regulates trichome differentiation and anthocyanin biosynthesis in Arabidopsis, encodes a WD40 repeat protein. *Plant Cell* **11**, 1337–1349 (1999).
30. Payne, C. T., Zhang, F. & Lloyd, A. M. *GL3* encodes a bHLH protein that regulates trichome development in Arabidopsis through interaction with GL1 and TTG1. *Genetics* **156**, 1349–1362 (2000).
31. Zhang, F., Gonzalez, A., Zhao, M., Payne, C. T. & Lloyd, A. A network of redundant bHLH proteins functions in all TTG1-dependent pathways of *Arabidopsis*. *Development* **130**, 4859–4869 (2003).
32. Yao, X. et al. The making of elaborate petals in *Nigella* through developmental repatterning. *New Phytol.* **223**, 385–396 (2019).
33. Weber, A. Pollination of *Nigella arvensis* (Ranunculaceae) (film presentation). *Plant Syst. Evol.* **9**, 325–326 (1995).
34. Wang, P. et al. Flexibility in the structure of spiral flowers and its underlying mechanisms. *Nat. Plants* **2**, 15188 (2016).

35. Liao, H. et al. The morphology, molecular development and ecological function of pseudonectaries on *Nigella damascena* (Ranunculaceae) petals. *Nat. Commun.* **11**, 1777 (2020).
36. Zhang, R. et al. Identification of the key regulatory genes involved in elaborate petal development and specialized character formation in *Nigella damascena* (Ranunculaceae). *Plant Cell* **32**, 3095–3112 (2020).
37. Yuan, Y. et al. Mechanisms underlying the formation of complex color patterns on *Nigella orientalis* (Ranunculaceae) petals. *New Phytol.* **237**, 2450–2466 (2023).
38. Melaragno, J. E., Mehrotra, B. & Coleman, A. W. Relationship between endopolyploidy and cell size in epidermal tissue of Arabidopsis. *Plant Cell* **5**, 1661–1668 (1993).
39. Zaitoun, S., Al-Ghzawi, A. A., Samarah, N. & Alqudah, A. Comparative study in seed yield and flowers attractivity to bee visitors between *Nigella sativa* L. and *Nigella damascena* L. (Ranunculaceae) grown under semiarid conditions. *Ital. J. Agron.* **2**, 125–130 (2008).
40. Zhao, H. et al. Delphinieae flowers originated from the rewiring of interactions between duplicated and diversified floral organ identity and symmetry genes. *Plant Cell* **35**, 994–1012 (2023).
41. Gonzalez, A., Mendenhall, J., Huo, Y. & Lloyd, A. TTG1 complex MYBs, MYB5 and TT2, control outer seed coat differentiation. *Dev. Biol.* **325**, 412–421 (2009).
42. Cavallini, E. et al. Functional diversification of grapevine MYB5a and MYB5b in the control of flavonoid biosynthesis in a petunia anthocyanin regulatory mutant. *Plant Cell Physiol.* **55**, 517–534 (2014).
43. Liu, C., Jun, J. H. & Dixon, R. A. MYB5 and MYB14 play pivotal roles in seed coat polymer biosynthesis in *Medicago truncatula*. *Plant Physiol.* **165**, 1424–1439 (2014).
44. Shan, X. et al. Molecular insights into TT2-Type MYB regulators illuminate the complexity of floral flavonoids biosynthesis in *Freesia hybrida*. *Hortic. Res.* **12**, uhae1352 (2025).
45. Li, S. F. et al. The *Arabidopsis* MYB5 transcription factor regulates mucilage synthesis, seed coat development, and trichome morphogenesis. *Plant Cell* **21**, 72–89 (2009).
46. Wang, N. et al. Genetic variation in *MYB5_A12* is associated with fibre initiation and elongation in tetraploid cotton. *Plant Biotechnol. J.* **19**, 1892–1894 (2021).
47. Tian, Y. & Zhang, T. MIXTAs and phytohormones orchestrate cotton fiber development. *Curr. Opin. Plant Biol.* **59**, 101975 (2021).
48. Wu, M. et al. A HD-ZIP transcription factor specifies fates of multicellular trichomes via dosage-dependent mechanisms in tomato. *Dev. Cell* **58**, 278–288 (2023).
49. Chang, J. et al. Spatiotemporal formation of glands in plants is modulated by MYB-like transcription factors. *Nat. Commun.* **15**, 2303 (2024).
50. Zumajo-Cardona, C. et al. Evolutionary studies of the bHLH transcription factors belonging to MBW complex: their role in seed development. *Ann. Bot.* **132**, 383–400 (2023).
51. Jiang, C. K. & Rao, G. Y. Insights into the diversification and evolution of R2R3-MYB transcription factors in plants. *Plant Physiol.* **183**, 637–655 (2020).
52. Nesi, N. et al. The *TT8* gene encodes a basic helix-loop-helix domain protein required for expression of *DFR* and *BAN* genes in Arabidopsis siliques. *Plant Cell* **12**, 1863–1878 (2000).
53. Xu, W. et al. Regulation of flavonoid biosynthesis involves an unexpected complex transcriptional regulation of *TT8* expression, in Arabidopsis. *New Phytol.* **198**, 59–70 (2013).
54. Li, P. et al. Regulation of anthocyanin and proanthocyanidin biosynthesis by *Medicago truncatula* bHLH transcription factor MtTT8. *New Phytol.* **210**, 905–921 (2016).
55. Maes, L., Inzé, D. & Goossens, A. Functional specialization of the TRANSPARENT TESTA GLABRA1 network allows differential hormonal control of laminal and marginal trichome initiation in Arabidopsis rosette leaves. *Plant Physiol.* **148**, 1453–1464 (2008).
56. Wang, L. et al. A spatiotemporally regulated transcriptional complex underlies heteroblastic development of leaf hairs in *Arabidopsis thaliana*. *EMBO J.* **38**, e100063 (2019).
57. Zhang, H. et al. The mechanism underlying asymmetric bending of lateral petals in *Delphinium* (Ranunculaceae). *Curr. Biol.* **34**, 755–768 (2024).
58. Wu, M. et al. HD-Zip proteins modify floral structures for self-pollination in tomato. *Science* **384**, 124–130 (2024).
59. El Ottra, J. H. L., Pirani, J. R. & Endress, P. K. Fusion within and between whorls of floral organs in Galipeinae (Rutaceae): structural features and evolutionary implications. *Ann. Bot.* **111**, 821–837 (2013).
60. Lam, T., Ho, Y. & Chen, S. Observations on ultraviolet-fluorescent trichomes on the tepals of *Narcissus* flowers. *Plant Sci. Lett.* **18**, 115–120 (1980).
61. Ågren, L., Kullenberg, B. & Sensenbaugh, T. Congruences in pilosity between three species of *Ophrys* (Orchidaceae) and their hymenopteran pollinators. *Nova Acta Reg. Soc. Sci. Ups. Ser. V:C* **3**, 15–25 (1984).
62. Jordan, G. J., Weston, P. H., Carpenter, R. J., Dillon, R. A. & Brodribb, T. J. The evolutionary relations of sunken, covered, and encrypted stomata to dry habitats in Proteaceae. *Am. J. Bot.* **95**, 521–530 (2008).
63. Robinson, D. O. et al. Ploidy and size at multiple scales in the Arabidopsis sepal. *Plant Cell* **30**, 2308–2329 (2018).
64. Zhang, J. & Feng, M. A plant sample optimal pretreatment for flow cytometric analysis. *Chin. Bull. Bot.* **58**, 285–297 (2023).
65. Li, B. & Dewey, C. N. RSEM: accurate transcript quantification from RNA-Seq data with or without a reference genome. *BMC Bioinforma.* **12**, 323 (2011).
66. Thompson, J. D., Gibson, T. J., Plewniak, F., Jeanmougin, F. & Higgins, D. G. The CLUSTAL_X windows interface: flexible strategies for multiple sequence alignment aided by quality analysis tools. *Nucleic Acids Res.* **25**, 4876–4882 (1997).
67. Kumar, S., Stecher, G., Li, M., Knyaz, C. & Tamura, K. MEGA X: molecular evolutionary genetics analysis across computing platforms. *Mol. Biol. Evol.* **35**, 1547–1549 (2018).
68. Nguyen, L. T., Schmidt, H. A., Von Haeseler, A. & Minh, B. Q. IQ-TREE: a fast and effective stochastic algorithm for estimating maximum-likelihood phylogenies. *Mol. Biol. Evol.* **32**, 268–274 (2015).

## Acknowledgments

We thank Guixia Xu, Yang Dong, Minliang Wu, and Kong laboratory members for their valuable comments and helpful discussions. This work was supported by grants from the National Natural Science Foundation of China (32221001 and 32200185) and the Chinese Academy of Sciences (ZDBS-LY-SM022).

## Author contributions

C.P., X.F., X.Yao, H.K. and H.S. designed the research. C.P. performed morphological and histological studies with the help of X.Yao and J.C.; C.P. analyzed the RNA-seq data and performed statistical analyses with the help of X.F. and Y.Y.; C.P. conducted mRNA in situ hybridization, VIGS experiments and qRT-PCR with the help of H.L. and X.L.; S.L. performed pollination studies; C.P. conducted phylogenetic analyses with the help of X.F. and H.S.; C.P., X.Yao, X.F., S.L., X.Yin, H.K. and H.S. wrote the manuscript, with contributions from all co-authors.

## Competing interests

The authors declare no competing interests.

## Additional information

**Supplementary information** The online version contains supplementary material available at https://doi.org/10.1038/s41467-025-64028-3.

**Correspondence** and requests for materials should be addressed to Hongzhi Kong or Hongyan Shan.

**Peer review information** *Nature Communications* thanks Laura Serna and Verónica Di Stilio for their contribution to the peer review of this work. A peer review file is available.